Exploring the Potential of AlphaFold Distograms for Flexibility Assignment in Cryo-EM Maps

Büşra Savaş[1,2], Ayşe Berçin Barlas[1], Ezgi Karaca[1,2]

[1]İzmir Biomedicine and Genome Center, İzmir, Türkiye; [2]Izmir International Biomedicine and Genome Institute, Dokuz Eylül University, Izmir, Türkiye

Corresponding Author: Ezgi Karaca (ezgi.karaca@ibg.edu.tr)

Abstract

AlphaFold (AF) models are widely used in cryo-EM workflows, but their static structure predictions limit the interpretation of flexible or unresolved regions. To address this, we investigate whether AF-generated distance probability distributions (distograms) can reveal conformational flexibility, using the AIFM1/AK2 complex as a test case. Molecular dynamics simulations identified a hinge-driven motion in AK2 upon AIFM1 binding, which was accurately reflected in distograms from AF2.3 and AF3, though not in their predicted structures. Enhanced sampling and MSA perturbations did not improve flexibility detection in earlier AF2 versions. So, by analyzing a key metabolic complex, we demonstrate that distograms might offer a promising approach for structure-free identification of flexible protein regionsl for interpreting dynamic signals in cryo-EM maps.

Key words: AlphaFold, Distogram, Cryo-EM, Conformational flexibility, Hinge motion, Multiple sequence alignment

Word count: 119

Introduction

Before AlphaFold2 (AF2) transformed structure prediction, identifying and modeling protein–protein interactions within low-resolution cryo-electron microscopy (cryo-EM) maps primarily relied on integrative approaches. These methods combined partial structural models with spatial restraints obtained from experimental techniques such as cross-linking mass spectrometry [1-3]. Integrative strategies were particularly effective for assigning the subcomplexes in large, dynamic assemblies [4-6]. The release of AF2 significantly advanced this process by allowing direct prediction of monomer and subcomplex structures that could directly be fitted into cryo-EM maps to guide model building [7]. A prominent example is the structural annotation of the human nuclear pore complex, where AF2 predictions successfully accounted for cryo-EM density across this exceptionally large macromolecular assembly (from *Xenopus laevis*, PDB ID: 7TDZ)[8].

Despite these advances, AF2 still has limitations in modeling structural flexibility. AF-predicted models fit well in regions of proteins and complexes that are clearly resolved in EM maps. However, they are more difficult to interpret in areas with missing or ambiguous densities, especially in protein regions undergoing large conformational changes upon binding **[9-12]**. This limitation stems from AF2's architecture, which is designed to converge on a single static structure for each input sequence [7]. To address this limitation, several tools have been developed that repurpose AF as a conformational sampler to explore large-scale rearrangements in protein structures [13-17]. These methods manipulate the input multiple sequence alignment (MSA), by masking specific residue positions (columns) or sequences (rows), to uncover alternative protein conformations [18,19]. Alternatively, they guide sampling toward functional conformations, such as open or closed, by incorporating structural templates from homologous proteins that are captured in those states [20,21]. Although these strategies can generate diverse structural ensembles, a key limitation remains: it is often unclear which model best represents the biologically or experimentally desired conformation. In this context, a tool that can rapidly identify protein regions prone to experience large conformational changes upon binding would be highly valuable. Such predictions could, for example, allow proteins to be segmented into rigid domains that can be fitted independently into EM maps. This approach is conceptually similar to the flexible multidomain docking strategy introduced in HADDOCK nearly fifteen years ago [22].

To advance flexibility-aware structural interpretation, we highlight a key observation by Schwarz et al. (2021), who showed that residue-level flexibility estimated from molecular dynamics (MD) simulations closely correlates with the pairwise distance probability profiles derived from *distograms* [23]. Distograms were first introduced in CASP13 with AF1, where a convolutional neural network was trained to convert MSA and template features into predicted distance probability distributions for all residue pairs [24]. In their study, Schwarz et al. showed that multimodal distance profiles, those with multiple probability peaks, tend to occur in flexible regions and may indicate domain motions or structural rearrangements. In contrast, unimodal profiles with a single sharp peak are typically associated with rigid segments within the protein. Building on this insight, here, we investigate whether distograms generated by AF can aid in interpreting flexible regions in the cryo-EM maps. As a test case, we focused on a recently

published cryo-EM structure of adenylate kinase 2 (AK2) in complex with apoptosis-inducing factor (AIFM1), a key metabolic complex involved in the apoptogenic signaling of mitochondria [25]. In this complex, AK2 undergoes a previously uncharacterized, binding-induced conformational change that includes both a hinge-like motion and a local structural rearrangement. To assess whether this flexibility is captured by AF-derived distograms, we followed the approach of Schwarz et al., using MD simulations as a reference. Specifically, we compared the key distance fluctuations observed in the MD trajectories with the inter-residue distance probability distributions predicted by the distogram outputs of AF2 and the recently released AF3 [7,26]. All related input and output files, figure-generation code, and additional scripts are available at https://github.com/CSB-KaracaLab/af-distogram-flexibility.

Results

A Key Metabolic Complex as a Proof-of-Concept for Distogram-Based Flexibility Detection

AK2 is a mitochondrial isoform of the adenylate kinase enzyme family, responsible for maintaining cellular energy homeostasis. It catalyzes the reversible phosphorylation of AMP to ADP using ATP [27,28]. With this, AK2 controls adenine nucleotide levels in the intermembrane space. Like other adenylate kinases, AK2 undergoes substantial domain motions during its catalytic cycle [29-31]. By interacting with AIFM1, AK2 modulates redox-sensitive conformation of AIFM1, acting as a molecular switch between metabolic homeostasis and caspase-independent cell death [25,32]. Beyond its well-characterized domain motions, AK2 also exhibits a binding-induced conformational change not captured in the previously resolved structures of this family. Two recent cryo-EM structures of the human AIFM1/AK2 complex reveal that the flexible C-terminal region of AK2, which is absent in the crystal structure of free AK2 (PDB ID: 2C9Y), adopt a β-strand conformation that stacks against the C-terminal domain of AIFM1 [25,32,33]. In one of these structures, Schildhauer et al. used AF3 to model the complex and successfully fit the predicted β-strand interaction into the EM density (PDB ID: 9FL7; overall resolution: 4.3 Å; local resolution at the stacking site: ~5 Å). This finding was independently validated by Rothemann et al., where the last eight C-terminal residues of AK2 are resolved, forming the β-stacking interface (PDB ID: 9GR0; overall resolution: 2.6 Å; local resolution: up to 3.2 Å) [32].

To evaluate whether this known structural transition is captured by AF models, we examined how AF2 and AF3 handle the flexible C-terminal region of AK2. Consistent with the crystal structure of the apo form, both models predicted this region with low confidence, reflected by a mean pLDDT score of 54 (Figure 1A). Notably, despite the absence of a relevant template, both AF2 and AF3 successfully modeled the C-terminal β-strand stacking against AIFM1 with high confidence (mean pLDDT: 77.6; Figure 1B), in agreement with the published holo structure. A comparison of the predicted apo and holo models revealed a substantial conformational shift at the C-terminus, with a root mean square deviation (RMSD) of 12 Å across the terminal residues. In particular, the Cβ–Cβ distance between residues 230 and 233 increased from 6.2 Å in the apo model to 10.5 Å in the holo model, capturing the key hinge-driven rearrangement observed in the AIFM1/AK2 complex. Because this distance best reflects the conformational change (Figure S1), we use the 230–233 residue pair as a marker to track this transition throughout the study.

Next, as a reference for ground truth, we monitored the marker distance between residues 230 and 233 using MD simulations. For the holo state, we relied on the previously published 4 μs all-atom MD trajectories of the AIFM1/AK2 complex (Figure 2A) [25,34]. To provide a comparative baseline, we conducted 4 μs of new MD simulations for apo AK2 using the same protocol described in that study. In the apo simulations, the marker distance predominantly ranged between 5.0 and 10.2 Å, with only ~1.7% of frames exceeding 7.6 Å, which is the minimum distance observed in the holo trajectory (Figure 2A, left). In contrast, the holo simulations showed a broader distribution from 7.6 to 13.3 Å, with a clear peak near

10 Å, consistent with the stabilized β-stacking conformation reported earlier (Figure 2B, left). For subsequent analysis, we used the median Cβ–Cβ distances from the MD simulations as reference thresholds: 6.0 Å (with a probability of 0.4) for the apo state and 10.0 Å (with a probability of 0.2) for the holo state.

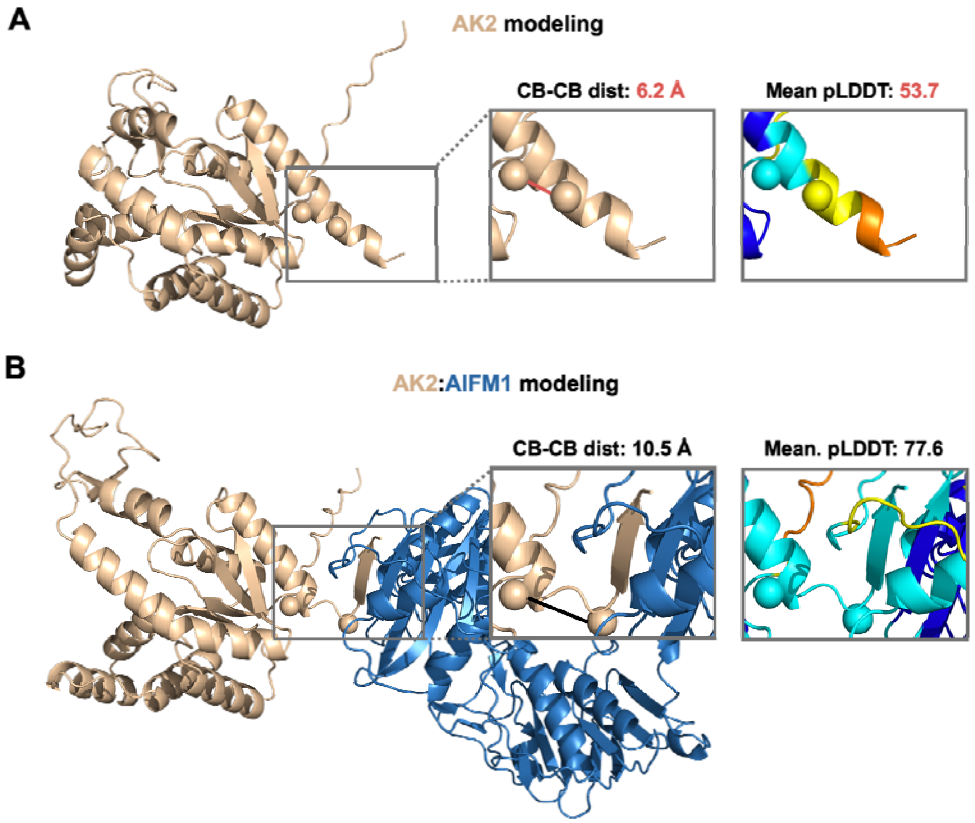

Figure 1. AlphaFold3 models capture a hinge-driven conformational switch of AK2. Top-ranked AF3 predictions (among 25 models) for apo **(A)** and holo **(B)** states of AK2 are shown. AK2 is depicted in wheat and AIFM1 in blue**.** Residues 230 and 233 of AK2, located at the flexible C-terminal end, are highlighted as spheres. Insets show close-up views of the Cβ–Cβ marker distance, together with the mean Cβ pLDDT scores of the last ten residues. pLDDT coloring indicates model confidence, with blue representing high and orange low confidence.

Distogram Profile Evolution Across AlphaFold Versions

To assess how accurately different AF versions reflect the conformational dynamics captured in our MD simulations, we compared our MD-based marker distance distributions with those predicted by the distograms of AF2 and AF3. For this, we generated 25 independent distance probability distributions by each model using identical MSA inputs to ensure consistent coevolutionary signals.The MSA was constructed using MMseqs2 via ColabFold, and model generation followed the default settings of AF2.0 (alphafold_ptm) and AF3 models (see SI for details)[35,36]. As an outcome, in the apo state, AF2 generated broad, bimodal distograms with peaks centered near ~6 Å and ~10 Å (Figure 2A). These peaks correspond approximately to the median distances observed in apo and holo MD simulations, respectively. However, the

distinction between the two peaks was limited, with the holo-associated peak reaching a probability of no more than 0.1. In contrast, AF3 produced distograms that closely mirrored the apo MD distribution in both peak positions and relative magnitudes, showing a striking agreement with the simulation data (Figure 2A). Upon modeling the holo complex (i.e., with AIFM1 present), the AF3 distograms transitioned to a unimodal distribution centered around the holo-state median (~10 Å), in line with the β-strand stacking conformation seen in the MD simulations (Figure 2B). AF2, on the other hand, retained a bimodal profile even in the holo condition, with only 3 of the 25 predictions displaying a unimodal peak comparable to those from AF3 (Figure 2B, middle).

To further examine how different AF2 configurations influence distogram outputs, we used our in-house sampling pipeline, MinnieFold, which systematically explores structural variability across the four major AF2 versions (ptm, v2.1, v2.2, and v2.3) [37-39]. Inspired by the Massive Sampling approach [16], MinnieFold systematically varies key AF2 sampling parameters such as the number of recycling steps, dropout settings, and template inclusion. It generates a total of 480 models across all four AF2 versions, enabling broad sampling of structural diversity in a computationally efficient manner. In the blind protein complex prediction challenge CAPRI55, we demonstrated that MinnieFold can produce interaction ensembles exhibiting up to 11.7 Å RMSD variation. Here, we applied MinnieFold to investigate how enhanced sampling affects distogram outputs, using the same input MSA as in our earlier AF2 and AF3 predictions (see SI text). The resulting distance distributions showed a mix of peak profiles, combining features seen in both AF2-ptm and AF3 (Figure 2C). When analyzed individually (Figure S2), ptm and v2.1 displayed similar broad bimodal profiles, with v2.1 showing a stronger apo-associated peak, indicating a tendency toward the unbound state. In contrast, v2.2 produced sharply unimodal distributions centered around 6.0 Å, with a high probability (~0.6). Notably, v2.3 reproduced a bimodal distribution closely matching the MD and AF3 profiles. These results suggest that increased sampling through MinnieFold does not introduce new flexibility signals beyond those observed in standard AF2 runs, but it can help amplify existing conformational features already encoded in specific versions.

Since parameter tuning alone did not introduce substantial diversity in the distogram outputs of AF2, we next examined the influence of the input MSA on flexibility prediction. To systematically assess how sequence diversity affects distogram behavior, we applied two orthogonal strategies. The first was AFsample2, which introduces stochasticity by randomly masking columns in the MSA to perturb coevolutionary signals [ref]. The second was AF_cluster, which clusters sequences to build reduced MSAs that represent distinct evolutionary subspaces [ref]. Both strategies were implemented using the ptm model for consistency. In the case of AFsample2, the overall bimodal character of the distograms was preserved, but the probability of the apo-associated distance peak approximately doubled compared to the original AF2 run (Figure 2A, D). In contrast, AF_cluster produced a distinct unimodal peak centered around 8 Å with a probability of approximately 0.15, in addition to the original apo and holo peaks observed in AF2 (Figure 2D). This intermediate peak may represent a false positive, resulting from reduced MSA depth or limited sequence diversity, or it could reflect a true transition state between the apo and holo conformations.

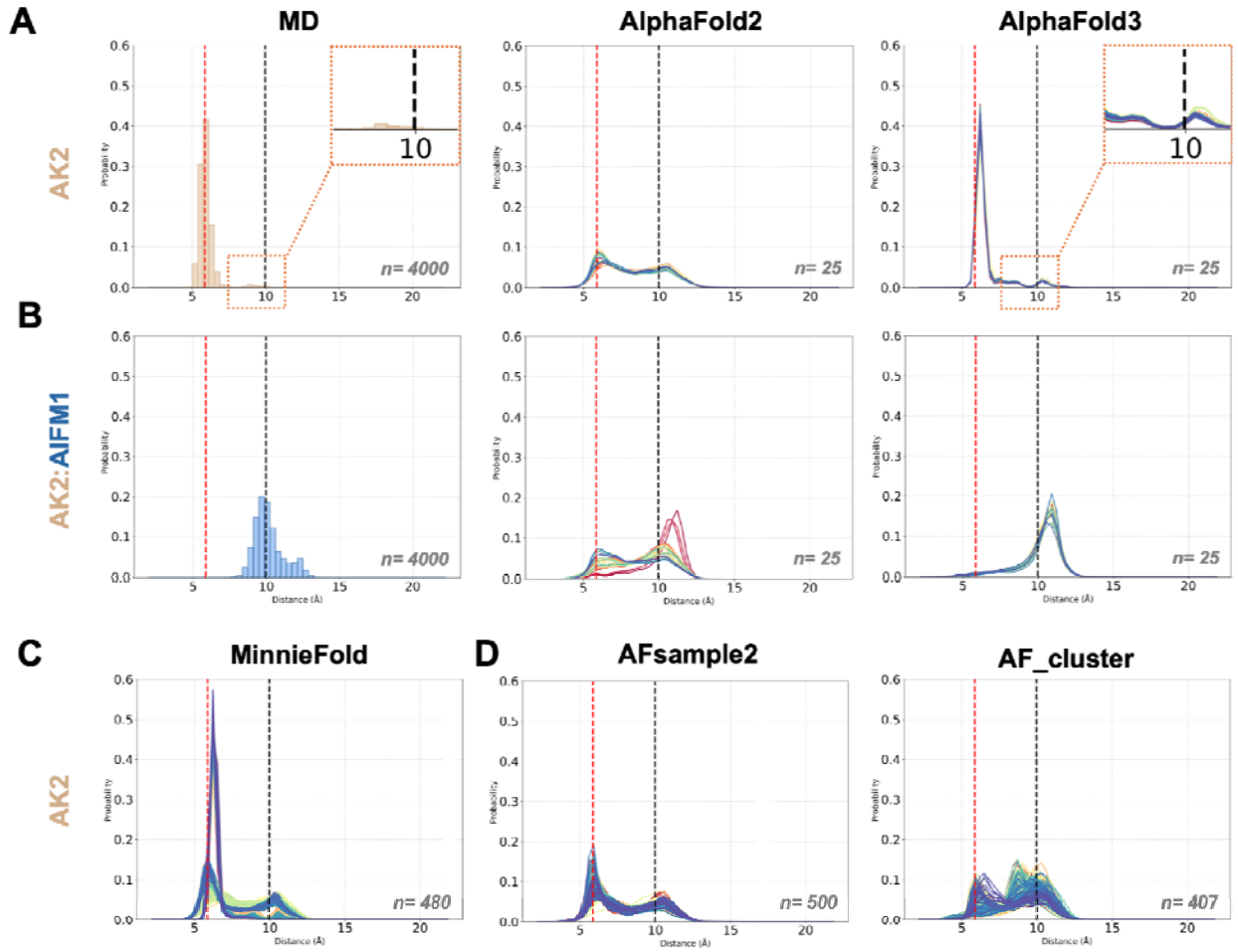

Figure 2. Comparison of marker hinge motion distances for AK2 and AIFM1/AK2. Distogram profiles of the predicted 230-233 marker distance of **(A)** apo and **(B)** AIFM1-bound AK2. Left: The measured distance probability distribution, obtained from MD simulations. Middle: AF2 distogram for the same pair. Right: AF3 distogram for the same pair. Distogram profiles of 230-233 pair calculated by (**C)** MinnieFold, (**D)** AFsample2 and AF_Cluster. The dashed lines indicate the threshold distances obtained from MD simulations: at 6.0 Å in red for the apo and 10.0 Å in black for the holo state. The sample given each plot is provided on the pane, indicated with *n.*

Discussion

In this Perspective article, we investigate whether AF-generated distograms can capture functionally relevant conformational flexibility. For this, we focus on a hinge-driven structural change in AK2 upon AIFM1 binding. Our aim is to assess whether distance probability profiles from distograms reflect the conformational landscape observed in MD simulations and whether they offer practical value for interpreting flexible regions in cryo-EM maps.

Our results show that both AF2.3 and AF3 closely reproduce the hinge dynamics at the C-terminal region of AK2, aligning surprisingly well with distance distributions derived from MD simulations. This is a significant finding, especially given that the ensembles of predicted models from AF2.3 or AF3 do not reflect this behavior, likely because AF models are designed to converge toward high-probability structural states (Figure S3). So, distogram profiles may capture conformational heterogeneity more sensitively than AF's final structural predictions. Although additional studies are needed to generalize this observation, our current results support the potential of distogram profiles as a computational tool for identifying flexible regions. Such an insight could help inform downstream modeling workflows by flagging areas likely to undergo conformational change, enabling targeted sampling or flexible fitting in structural interpretation.

We next investigated whether alternative sampling strategies could improve the agreement between AF2-generated distograms and MD-derived reference distograms, particularly in cases where the generated distograms failed to capture the observed conformational variability. While previous studies have shown that such strategies can increase structural diversity in AF outputs, we found that they did not significantly change the distogram profiles. For example, masking specific columns in the MSA did not change the distogram profile beyond what was seen with standard AF2 sampling. This suggests that AF version differences, rather than sampling parameter tuning, have a larger influence on distogram behavior, particularly in modulating peak amplitudes. In contrast, changing MSA depth through sequence clustering, as implemented in AF_cluster, did produce distinct distogram profiles. This aligns with findings from Audagnotto et al. [40], who showed that MSA generation strategies can lead to either unimodal or bimodal distance distributions depending on sequence diversity. In our case, the MMseqs2-generated MSAs were sufficiently diverse to capture hinge-associated AK2 flexibility. However, identifying more subtle or transient conformational states may require further optimization of the input MSA. Since coevolutionary signal strength is sensitive to both the depth and diversity of the MSA, using multiple sequence databases or alignment methods could enrich MSAs with distant homologs. These improvements could enhance the ability of distograms to reflect biologically relevant flexibility. Nonetheless, confirming the functional relevance of such alternative states will ultimately require experimental validation, such as through NMR, as also emphasized in the original AF_cluster study.

Given the promising flexibility signals detected in AF2.3 and AF3, a key question arises: how can these distogram-based observations be effectively translated into structural data? One

notable step in this direction is the implementation of BioEmu, which feeds the pairwise embeddings from AF2 (alphafold_ptm) into a diffusion-based generative model to sample MD-like conformations [41]. Although pairwise embeddings are not explicit distograms, they encode similar spatial information. More recently, Boltz2 incorporated distogram-guided sampling into its generative pipeline [42]. In comparative benchmarks against BioEmu using MD datasets, Boltz2 showed superior performance, further supporting our findings with alphafold_ptm. This raises an intriguing possibility: could pairwise representations from AF3 or AF2.3 enhance the performance of tools like BioEmu? Exploring this question represents a promising avenue for future development. Further support for distogram-based modeling is also growing within the structural biology community. Methods such as BAIes and AlphaFold-Metainference incorporate predicted distance distributions as probabilistic restraints in physics-based sampling [43–45]. These strategies have been particularly effective in modeling the dynamics of intrinsically disordered proteins (IDPs), highlighting the value of distogram-derived information in capturing structural flexibility.

Ultimately, our findings support a growing consensus that distograms offer a unique and underutilized window into conformational insight. With the right computational tools, ranging from simple visual inspection to advanced generative models, it is possible to uncover meaningful conformational dynamics that escape AI-based structure prediction. We hope this work encourages further efforts to develop distogram-informed frameworks, particularly for the interpretation of dynamic metabolic assemblies in low-resolution cryo-EM datasets. To aid such studies, we share our MSA files, distogram outputs, predicted PDB structures, as well as the code used to generate the figures in this manuscript at https://github.com/CSB-KaracaLab/af-distogram-flexibility .

REFERENCES

1. Karaca, E., & Bonvin, A. M. (2013). Advances in integrative modeling of biomolecular complexes. Methods (San Diego, Calif.), 59(3), 372–381. https://doi.org/10.1016/j.ymeth.2012.12.004
2. Bullock, J. M. A., Sen, N., Thalassinos, K., & Topf, M. (2018). Modeling Protein Complexes Using Restraints from Crosslinking Mass Spectrometry. Structure (London, England : 1993), 26(7), 1015–1024.e2. https://doi.org/10.1016/j.str.2018.04.016
3. Graziadei, A., & Rappsilber, J. (2022). Leveraging crosslinking mass spectrometry in structural and cell biology. Structure (London, England : 1993), 30(1), 37–54. https://doi.org/10.1016/j.str.2021.11.007
4. Karaca, E., Rodrigues, J. P. G. L. M., Graziadei, A., Bonvin, A. M. J. J., & Carlomagno, T. (2017). M3: an integrative framework for structure determination of molecular machines. Nature methods, 14(9), 897–902. https://doi.org/10.1038/nmeth.4392
5. Skalidis, I., Kyrilis, F. L., Tüting, C., Hamdi, F., Chojnowski, G., & Kastritis, P. L. (2022). Cryo-EM and artificial intelligence visualize endogenous protein community members. Structure (London, England : 1993), 30(4), 575–589.e6. https://doi.org/10.1016/j.str.2022.01.001
6. Träger, T. K., Tüting, C., & Kastritis, P. L. (2024). The human touch: Utilizing AlphaFold 3 to analyze structures of endogenous metabolons. Structure (London, England : 1993), 32(10), 1555–1562. https://doi.org/10.1016/j.str.2024.08.018
7. Jumper, J., Evans, R., Pritzel, A., Green, T., Figurnov, M., Ronneberger, O., Tunyasuvunakool, K., Bates, R., Žídek, A., Potapenko, A., Bridgland, A., Meyer, C., Kohl, S. A. A., Ballard, A. J., Cowie, A., Romera-Paredes, B., Nikolov, S., Jain, R., Adler, J., Back, T., … Hassabis, D. (2021). Highly accurate protein structure prediction with AlphaFold. Nature, 596(7873), 583–589. https://doi.org/10.1038/s41586-021-03819-2
8. Fontana, P., Dong, Y., Pi, X., Tong, A. B., Hecksel, C. W., Wang, L., Fu, T. M., Bustamante, C., & Wu, H. (2022). Structure of cytoplasmic ring of nuclear pore complex by integrative cryo-EM and AlphaFold. *Science (New York, N.Y.)*, *376*(6598), eabm9326. https://doi.org/10.1126/science.abm9326
9. Saldaño, T., Escobedo, N., Marchetti, J., Zea, D. J., Mac Donagh, J., Velez Rueda, A. J., Gonik, E., García Melani, A., Novomisky Nechcoff, J., Salas, M. N., Peters, T., Demitroff, N., Fernandez Alberti, S., Palopoli, N., Fornasari, M. S., & Parisi, G. (2022). Impact of protein conformational diversity on AlphaFold predictions. *Bioinformatics (Oxford, England)*, *38*(10), 2742–2748. https://doi.org/10.1093/bioinformatics/btac202
10. Carugo, O. (2023). pLDDT Values in AlphaFold2 Protein Models Are Unrelated to Globular Protein Local Flexibility. Crystals, 13(11), 1560. https://doi.org/10.3390/cryst13111560
11. Del Alamo, D., Sala, D., Mchaourab, H. S., & Meiler, J. (2022). Sampling alternative conformational states of transporters and receptors with AlphaFold2. eLife, 11, e75751. https://doi.org/10.7554/eLife.75751
12. Guo, H. B., Perminov, A., Bekele, S., Kedziora, G., Farajollahi, S., Varaljay, V., Hinkle, K., Molinero, V., Meister, K., Hung, C., Dennis, P., Kelley-Loughnane, N., & Berry, R.

(2022). AlphaFold2 models indicate that protein sequence determines both structure and dynamics. Scientific reports, 12(1), 10696. https://doi.org/10.1038/s41598-022-14382-9

13. Cui, X., Ge, L., Chen, X., Lv, Z., Wang, S., Zhou, X., & Zhang, G. (2025). Beyond static structures: protein dynamic conformations modeling in the post-AlphaFold era. Briefings in bioinformatics, 26(4), bbaf340. https://doi.org/10.1093/bib/bbaf340

14. Stein, R. A., & Mchaourab, H. S. (2022). SPEACH_AF: Sampling protein ensembles and conformational heterogeneity with Alphafold2. PLoS computational biology, 18(8), e1010483. https://doi.org/10.1371/journal.pcbi.1010483

15. Wallner B. (2023). AFsample: improving multimer prediction with AlphaFold using massive sampling. Bioinformatics (Oxford, England), 39(9), btad573. https://doi.org/10.1093/bioinformatics/btad573

16. Raouraoua, N., Mirabello, C., Véry, T., Blanchet, C., Wallner, B., Lensink, M. F., & Brysbaert, G. (2024). MassiveFold: unveiling AlphaFold's hidden potential with optimized and parallelized massive sampling. Nature computational science, 4(11), 824–828. https://doi.org/10.1038/s43588-024-00714-4

17. Jing B, Berger B, Jaakkola A. (2024) AlphaFold Meets Flow Matching for Generating Protein Ensembles. Rxiv. https://doi.org/10.48550/arXiv.2402.04845

18. Kalakoti, Y., & Wallner, B. (2025). AFsample2 predicts multiple conformations and ensembles with AlphaFold2. Communications biology, 8(1), 373. https://doi.org/10.1038/s42003-025-07791-9

19. Wayment-Steele, H. K., Ojoawo, A., Otten, R., Apitz, J. M., Pitsawong, W., Hömberger, M., Ovchinnikov, S., Colwell, L., & Kern, D. (2024). Predicting multiple conformations via sequence clustering and AlphaFold2. Nature, 625(7996), 832–839. https://doi.org/10.1038/s41586-023-06832-9

20. Sala, D., Hildebrand, P. W., & Meiler, J. (2023). Biasing AlphaFold2 to predict GPCRs and kinases with user-defined functional or structural properties. Frontiers in molecular biosciences, 10, 1121962. https://doi.org/10.3389/fmolb.2023.1121962

21. Heo, L., & Feig, M. (2022). Multi-state modeling of G-protein coupled receptors at experimental accuracy. Proteins, 90(11), 1873–1885. https://doi.org/10.1002/prot.26382

22. Karaca, E., & Bonvin, A. M. (2011). A multidomain flexible docking approach to deal with large conformational changes in the modeling of biomolecular complexes. Structure (London, England : 1993), 19(4), 555–565. https://doi.org/10.1016/j.str.2011.01.014

23. Schwarz, D., Georges, G., Kelm, S., Shi, J., Vangone, A., & Deane, C. M. (2021). Co-evolutionary distance predictions contain flexibility information. Bioinformatics (Oxford, England), 38(1), 65–72. https://doi.org/10.1093/bioinformatics/btab562

24. Senior, A. W., Evans, R., Jumper, J., Kirkpatrick, J., Sifre, L., Green, T., Qin, C., Žídek, A., Nelson, A. W. R., Bridgland, A., Penedones, H., Petersen, S., Simonyan, K., Crossan, S., Kohli, P., Jones, D. T., Silver, D., Kavukcuoglu, K., & Hassabis, D. (2020). Improved protein structure prediction using potentials from deep learning. Nature, 577(7792), 706–710. https://doi.org/10.1038/s41586-019-1923-7

25. Schildhauer, F., Ryl, P. S. J., Lauer, S. M., Lenz, S., Barlas, A. B., Ouzounidis, V. R., Jeffrey, K., Marcu, D. C., O'Reilly, F. J., Graziadei, A., Stuiver, M., Schmidt, K., Ewers, H., Spahn, C. M. T., Karaca, E., Busch, K. E., Cheerambathur, D., Schwefel, D., &

Rappsilber, J. (2025). An NADH-controlled gatekeeper of ATP synthase. Molecular cell, 85(13), 2567–2580.e12. https://doi.org/10.1016/j.molcel.2025.06.007

26. Abramson, J., Adler, J., Dunger, J., Evans, R., Green, T., Pritzel, A., Ronneberger, O., Willmore, L., Ballard, A. J., Bambrick, J., Bodenstein, S. W., Evans, D. A., Hung, C. C., O'Neill, M., Reiman, D., Tunyasuvunakool, K., Wu, Z., Žemgulytė, A., Arvaniti, E., Beattie, C., … Jumper, J. M. (2024). Accurate structure prediction of biomolecular interactions with AlphaFold 3. Nature, 630(8016), 493–500. https://doi.org/10.1038/s41586-024-07487-w

27. Burkart, A., Shi, X., Chouinard, M., & Corvera, S. (2011). Adenylate kinase 2 links mitochondrial energy metabolism to the induction of the unfolded protein response. The Journal of biological chemistry, 286(6), 4081–4089. https://doi.org/10.1074/jbc.M110.134106

28. Dzeja, P., & Terzic, A. (2009). Adenylate Kinase and AMP Signaling Networks: Metabolic Monitoring, Signal Communication and Body Energy Sensing. International Journal of Molecular Sciences, 10(4), 1729-1772. https://doi.org/10.3390/ijms10041729

29. Formoso, E., Limongelli, V., & Parrinello, M. (2015). Energetics and structural characterization of the large-scale functional motion of adenylate kinase. Scientific reports, 5, 8425. https://doi.org/10.1038/srep08425

30. Snow, C., Qi, G., & Hayward, S. (2007). Essential dynamics sampling study of adenylate kinase: comparison to citrate synthase and implication for the hinge and shear mechanisms of domain motions. Proteins, 67(2), 325–337. https://doi.org/10.1002/prot.21280

31. Whitford, P. C., Gosavi, S., & Onuchic, J. N. (2008). Conformational transitions in adenylate kinase. Allosteric communication reduces misligation. The Journal of biological chemistry, 283(4), 2042–2048. https://doi.org/10.1074/jbc.M707632200

32. Rothemann, R. A., Pavlenko, E., Mondal, M., Gerlich, S., Grobushkin, P., Mostert, S., Racho, J., Weiss, K., Stobbe, D., Stillger, K., Lapacz, K., Salscheider, S. L., Petrungaro, C., Ehninger, D., Nguyen, T. H. D., Dengjel, J., Neundorf, I., Bano, D., Poepsel, S., & Riemer, J. (2025). Interaction with AK2A links AIFM1 to cellular energy metabolism. Molecular cell, 85(13), 2550–2566.e6. https://doi.org/10.1016/j.molcel.2025.05.036

33. 2C9Y X-ray structure, (2005). https://doi.org/10.2210/pdb2C9Y/pdb

34. Barlas, A.B. (2024). Understanding the function of biomolecular complexes through the lens of molecular dynamics. [Doctoral dissertation, Dokuz Eylul University, Izmir]. Source: https://tez.yok.gov.tr/UlusalTezMerkezi/TezGoster?key=E_eEUHQic_C-LvhxNQn1W3wmOCInlBnVAZxdJWqWdN5YkWRUeQ_5_WUDFHGmyRtK

35. Steinegger, M., & Söding, J. (2017). MMseqs2 enables sensitive protein sequence searching for the analysis of massive data sets. Nature biotechnology, 35(11), 1026–1028. https://doi.org/10.1038/nbt.3988

36. Mirdita, M., Schütze, K., Moriwaki, Y., Heo, L., Ovchinnikov, S., & Steinegger, M. (2022). ColabFold: making protein folding accessible to all. Nature methods, 19(6), 679–682. https://doi.org/10.1038/s41592-022-01488-1

37. Savaş, B., Yılmazbilek, İ., Özsan, A., & Karaca, E. (2025). Towards a Greener AlphaFold2 Protocol for Antibody-Antigen Modeling: Insights From CAPRI Round 55.

Proteins, 10.1002/prot.26820. Advance online publication. https://doi.org/10.1002/prot.26820

38. Evans R, O'Neill M, Pritzel A, Antropova N, Senior A, Green T, Žídek A, Bates R, Blackwell S, Yim J et al. (2022) Protein complex prediction with AlphaFold-multimer. bioRxiv. https://doi.org/10.1101/2021.10.04.463034

39. https://github.com/google-deepmind/alphafold/blob/main/docs/technical_note_v2.3.0.md AlphaFold v2.3 technical note, released after CASP15.

40. Audagnotto, M., Czechtizky, W., De Maria, L., Käck, H., Papoian, G., Tornberg, L., Tyrchan, C., & Ulander, J. (2022). Machine learning/molecular dynamic protein structure prediction approach to investigate the protein conformational ensemble. Scientific reports, 12(1), 10018. https://doi.org/10.1038/s41598-022-13714-z

41. Lewis, S., Hempel, T., Jiménez-Luna, J., Gastegger, M., Xie, Y., Foong, A. Y. K., Satorras, V. G., Abdin, O., Veeling, B. S., Zaporozhets, I., Chen, Y., Yang, S., Foster, A. E., Schneuing, A., Nigam, J., Barbero, F., Stimper, V., Campbell, A., Yim, J., Lienen, M., … Noé, F. (2025). Scalable emulation of protein equilibrium ensembles with generative deep learning. Science (New York, N.Y.), eadv9817. Advance online publication. https://doi.org/10.1126/science.adv9817

42. Passaro S, Corso G, Wohlwend J, Reveiz M, Thaler S, Somnath VR, Getz N, Portnoi T, Roy J, Stark H et al. (2025) Boltz-2: Towards Accurate and Efficient Binding Affinity Prediction. bioRxiv. https://doi.org/10.1101/2025.06.14.659707

43. Brotzakis, Z. F., Zhang, S., Murtada, M. H., & Vendruscolo, M. (2025). AlphaFold prediction of structural ensembles of disordered proteins. Nature communications, 16(1), 1632. https://doi.org/10.1038/s41467-025-56572-9

44. Schnapka, V., Morozova, T. I., Sen, S., & Bonomi, M. (2025). Atomic resolution ensembles of intrinsically disordered proteins with Alphafold. bioRxiv. https://doi.org/10.1101/2025.06.18.660298

45. Sen, S., Hoff, S.□E., Morozova, T.□I., Schnapka, V., & Bonomi, M. (2025). Advancing in silico drug design with Bayesian refinement of AlphaFold models. bioRxiv. https://doi.org/10.1101/2025.06.25.661454